

Technical Paper

Numerical simulation of soft longitudinal joints in concrete-faced rockfill dam

Mo-Zhen Zhou, Bing-yin Zhang, Yu-xin Jie*

State Key Laboratory of Hydroscience and Engineering, Sanjiangyuan Collaborative Innovation Center, Tsinghua University, Beijing 100084, China

Received 12 March 2015; received in revised form 26 August 2015; accepted 26 January 2016

Available online 6 May 2016

Abstract

In the construction of high concrete-faced rockfill dams (CFRDs), soft filler is used in the longitudinal joints in order to avoid extrusion damage to the concrete face slab. In this paper, we consider the soft joint contact as an equivalent contact interface to avoid introducing conventional elements. Based on the introduction of a general transformation to obtain fully decoupled contact constraints, a new generalized node-to-segment formulation is developed to solve the multi-body contact problem in CFRDs. The high CFRD of Tianshengqiao-1 in China is numerically analyzed; the results show that soft joints can significantly reduce the axial stress of face slabs.

© 2016 The Japanese Geotechnical Society. Production and hosting by Elsevier B.V. All rights reserved.

Keywords: High concrete-faced rockfill dam; Soft longitudinal joint; Transformation; Perturbed Lagrange method; Nonlinear contact

1. Introduction

The development of concrete-faced rockfill dams (CFRDs) has been rapid over the past two decades (Cooke, 1991). CFRDs can be built in different geological environments and climates, and the construction materials can be easily acquired. At present, the construction technologies of CFRDs with a height of 250 m or more are facing great challenges. Engineering experience from existing projects has shown that the main risk of high CFRDs is the potential failure of the concrete face slabs, especially the extrusion damage occurring in CFRDs higher than 150 m (Cao and Zhang, 2001). Fig. 1 is a photo of the extrusion damage to the concrete face slabs in the Tianshengqiao-1 CFRD project.

To prevent extrusion damage, compressible soft filler is generally used to fill the longitudinal joints between the face slabs (Cao and Zhang, 2001; Johannesson and Tohlang, 2007; Cao and Xu, 2009; Li and Yang, 2012). The soft filler can absorb axial extrusion displacement, thus improving the distribution of stress in the compressive region of the face slabs. Fig. 2 shows the schematic of a soft joint. The soft joint between two face slabs is generally narrow, and its stiffness may increase when axial extrusion develops until the joint is nearly closed. To simulate this problem numerically, thin solid elements must be generated to represent the filler, and then the contact relations of the slab–filler–slab and the filler–cushion need to be treated. However, this method is generally too complicated to implement.

A more convenient way to simulate this problem is to represent the filler and the related interface as a composite interface. Generally, an interface element method, such as the Goodman element (Goodman et al., 1968) or Desai's thin-layer element (Desai et al., 1984), can be used to simulate the

*Corresponding author. Tel./fax: +86 10 62785593.

E-mail address: jieyx@tsinghua.edu.cn (Y.-x. Jie).

Peer review under responsibility of The Japanese Geotechnical Society.



Fig. 1. Extrusion damage to concrete face slabs in Tianshengqiao-1 CFRD project.

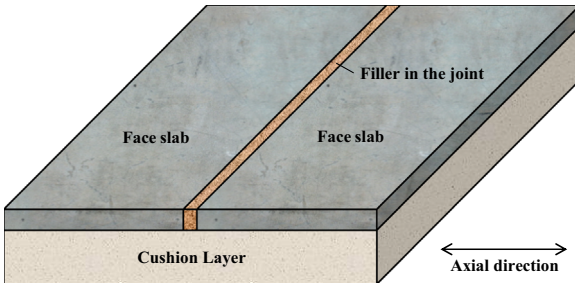


Fig. 2. Schematic of soft longitudinal joint.

interface in a CFRD numerical simulation using the finite element method (FEM) (Zhang et al., 2007; Arici, 2011; Kartal et al., 2012; Xu et al., 2012). However, researchers have indicated that it is difficult to obtain reasonable results with the interface element method when the discontinuous deformation is not small (Zhang et al., 2004; Qian et al., 2013). In particular, the interface element method generally leads to an ill-conditioned matrix system which may greatly influence the computational efficiency.

To overcome the drawbacks associated with the interface element method, the contact analysis method is a promising alternative. The node-to-segment (NTS) approach (Hallquist et al., 1985; Zhang et al., 2004; Sheng et al., 2006) and the segment-to-segment (STS) approach (Zavarise and Wriggers, 1998) are useful for simulating discontinuous deformation and for treating non-conforming meshes, and the NTS approach has been widely applied because of its simplicity. Nonlinear complementary contact constraints are imposed mainly by the penalty method, the Lagrange multiplier method, the perturbed Lagrange method or the augmented Lagrange method (Zavarise et al., 1995; Sitzmann et al., 2014).

In this paper, the interaction between the soft filler and the adjacent slabs is considered as an equivalent soft contact problem. Based on the introduction of a general transformation, we propose a new generalized NTS formulation, which includes the Lagrange multiplier formulation for hard contact problems and the perturbed Lagrange formulation for soft

contact problems. The transformation yields fully decoupled contact constraints. Therefore, in the Lagrange multiplier formulation, the Lagrange multipliers are condensed, and this prevents having to solve the saddle-point problem. In the perturbed Lagrange formulation, the penalty factor is only involved in the diagonal position of the matrix system; and thus, the ill-condition is overcome. The proposed generalized NTS formulation was used here to study the effect of soft joints on the extrusion of face slabs in the Tianshengqiao-1 CFRD.

This paper is organized as follows. In Section 2, we briefly introduce the theory of the NTS approach using the Lagrange multiplier method to impose the contact constraints. In Section 3, details of the new generalized NTS formulation are given, and a convenient estimation of the penalty factor is provided. Section 4 outlines the main features of the Tianshengqiao-1 hydropower project (TSQ-1 project) and presents a numerical study on the effect of soft joints on the axial extrusion stress of face slabs. Finally, conclusions are drawn in Section 5.

2. Node-to-segment approach

2.1. Description of contact problem

Fig. 3 shows the contact between two objects with finite deformation. The kinematic description of the contact problem involves domain Ω , which is composed of a master body Ω^m and a slave body Ω^s . The current configuration, \mathbf{x} (at time t), is described by reference configuration \mathbf{X} (at time 0) and a mapping $\varphi: \mathbf{x} = \varphi(\mathbf{X}, t)$. Thus, displacement \mathbf{u} can be written as $\mathbf{u}(\mathbf{X}, t) = \mathbf{x}(\mathbf{X}, t) - \mathbf{X}$. The current configurations in sub-domains Ω^m and Ω^s are denoted by \mathbf{x}^m and \mathbf{x}^s , respectively. The unit vectors in the normal and tangential directions to the master surface are denoted by \mathbf{n} and $\boldsymbol{\tau}$, respectively. Based on the normal vector, Fig. 3 also shows the projection method that yields the definition of the gap function in the normal direction, namely, $g = \mathbf{n} \cdot (\mathbf{x}^s - \mathbf{x}^m)$, where $g > 0$ means that the two bodies are separated, and vice versa.

If we denote the Neumann boundary by Γ^N and the Dirichlet boundary by Γ^D , the boundary value problem (BVP) can be

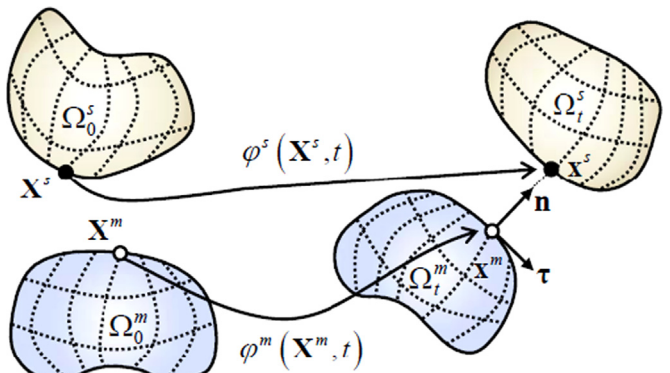


Fig. 3. Contact between two objects, illustrating two sub-domains, Ω^m and Ω^s , and projection method used in modeling.

written as follows:

$$\begin{aligned} \operatorname{div}(\boldsymbol{\sigma}) + \mathbf{b} &= \mathbf{0} && \text{in } \Omega, \\ \boldsymbol{\sigma} \mathbf{n}^N &= \circ \mathbf{t} && \text{on } \Gamma^N, \\ \mathbf{u} &= \circ \mathbf{u} && \text{on } \Gamma^D, \end{aligned} \quad (1)$$

where σ is the Cauchy stress tensor, \mathbf{b} represents the body forces, \mathbf{n}^N and $\circ \mathbf{t}$ are the current outward unit normal vector and the prescribed tractions on the Neumann boundary, respectively, and $\circ \mathbf{u}$ is the prescribed displacement on the Dirichlet boundary.

On the potential contact surface, Γ^C , the contact constraints in the normal direction can be summarized by the Hertz–Signorini–Moreau (HSM) condition as (Popp and Wall, 2014), namely,

$$g \geq 0, p_n \leq 0, \quad p_n g = 0, \quad (2)$$

where p_n is the contact traction in the normal direction. By introducing parameters ω and β , the frictional condition given by Coulomb's law can be written as the Karush–Kuhn–Tucker (KKT) condition (Popp and Wall, 2014) as follows:

$$\omega := \|\mathbf{t}_\tau\| - \mu |p_n|, \quad \bar{\mathbf{v}}_\tau + \beta \mathbf{t}_\tau = \mathbf{0}, \quad \omega \leq 0, \quad \beta \geq 0, \quad \omega \beta = 0, \quad (3)$$

where \mathbf{t}_τ is the tangential contact traction, μ is the coefficient of friction, $\bar{\mathbf{v}}_\tau$ is the tangential relative velocity, ω is the difference between the current value of friction and the maximum probable value of friction, and β represents the value of the tangential relative velocity per unit friction. The KKT condition generally describes the contact condition in the sticking state and the sliding state.

The treatment of the Neumann boundary and the Dirichlet boundary can be found in the conventional FEM theory. The constrained variation principle employing the Lagrange multiplier method to impose the contact constraints is given by

$$\begin{aligned} \delta \Pi(\mathbf{u}, \lambda) &= \delta \Pi^{\text{int,ext}}(\mathbf{u}) + \delta \Pi^C(\mathbf{u}, \lambda) = 0, \\ \delta \Pi^C(\mathbf{u}, \lambda) &= \delta \Pi_u^C + \delta \Pi_\lambda^C, \\ \delta \Pi_u^C &= \int_{\Gamma^C} \lambda \cdot (\delta \mathbf{u}^s - \delta \mathbf{u}^m) d\Gamma, \end{aligned} \quad (4)$$

where $\delta \Pi^{\text{int,ext}}$ is the standard virtual work from internal and external forces, λ is the Lagrange multiplier, $\delta \Pi^C$ is the contact virtual work, and $\delta \Pi_u^C$ is the part related to the contact traction. The variation in contact constrains $\delta \Pi_\lambda^C$ will be discussed in Section 2.3; \mathbf{u}^s and \mathbf{u}^m are the displacements of the slave node and the master node, respectively.

2.2. Spatial discretization

In this paper, the discretization of the displacement space is performed by FEM. The employed elements in domains Ω^m and Ω^s are eight-node linear isoparametric elements, and the resulting surface segments on the contact interfaces are four-node linear isoparametric elements. The discrete displacement is given by

$$\mathbf{x} \approx \mathbf{x}^h = \sum_{k=1}^{n^e} N_k \Big|_{\mathbf{x}^h} \mathbf{x}_k, \quad \mathbf{u} \approx \mathbf{u}^h = \sum_{k=1}^{n^e} N_k \Big|_{\mathbf{x}^h} \mathbf{d}_k, \quad (5)$$

where n^e is the number of nodes per element, N_k is the shape function with regard to the current approximate configuration, \mathbf{x}^h , and k denotes the local serial number of the node. The superscript h indicates that the corresponding quantity is an approximation defined in the discrete space and \mathbf{d} is the discrete nodal displacement. Matrix \mathbf{N} , composed of shape functions N_j , is defined as

$$\mathbf{N} = \begin{bmatrix} N_1 \mathbf{I}_3 & N_2 \mathbf{I}_3 & \cdots & N_{n_N} \mathbf{I}_3 \end{bmatrix}, \quad (6)$$

where n_N is the total node number of the domains and \mathbf{I}_3 is the identity matrix in $\mathbb{R}^{3 \times 3}$.

The discrete Lagrange multiplier is written as follows:

$$\lambda \approx \lambda^h = \psi \mathbf{z}, \quad \psi = \begin{bmatrix} \psi_1 \mathbf{I}_3 & \psi_2 \mathbf{I}_3 & \cdots & \psi_{n_\psi} \mathbf{I}_3 \end{bmatrix}, \quad (7)$$

where \mathbf{z} is the discrete nodal Lagrange multiplier, n_ψ is the total number of nodes in the discrete multiplier space, and matrix ψ is composed of shape functions ψ_j .

2.3. Treatment and discretization of contact constraints

The contact constraints represented by Eqs. (2) and (3) are inequality constraints that are complementary. In this paper, the primal–dual active set strategy (PDASS) (Hüeber and Wohlmuth, 2005) is employed to treat the contact constraints.

PDASS consists of finding and distinguishing different subsets from the slave nodes. All the nodes are divided into the master subset, \check{M} , the slave subset, \check{S} , and the remaining subset, \check{R} . Slave subset \check{S} is divided into the subset of inactive contacting nodes, \check{I} , and the subset of the active contacting nodes, \check{A} . Then, active subset \check{A} is further divided into the subset of the sticking nodes, \check{T} , and the subset of the sliding nodes, \check{L} .

The discrete Lagrange multipliers can be decomposed as

$$\mathbf{z}_j = z_j^n \mathbf{n}_j + \sum_{i=1}^2 z_j^{\tau_i} \{\boldsymbol{\tau}_i\}_j, \quad \forall \{j \in \check{A}\}, \quad (8)$$

where z_j^n and $z_j^{\tau_i}$ denote the normal and the tangential parts of the discrete Lagrange multipliers, respectively, and $\boldsymbol{\tau}_i$ denotes the tangential coordinate basis. As the Lagrange multipliers represent the contact tractions, we can insert the Lagrange multipliers into the contact constraints, and the discrete contact constraints can be determined by the partial derivative $\delta \Pi_\lambda^C / \delta \mathbf{z}$. In the NTS approach, the contact constraints are in a pointwise, strong form. The incremental form of the discrete contact constraints can then be written as

$$\mathbf{z}_j = \mathbf{0}, \quad \forall \{j \in \check{I}\}, \quad (9a)$$

$$\mathbf{n}_j \cdot \left(\Delta \mathbf{d}_j - \sum_{l=1}^{n_m^e} N_l \Big|_{\mathbf{x}_j^m} \Delta \mathbf{d}_l \right) = \Delta \circ g_j, \quad \forall \{j \in \check{A}\}, \quad (9b)$$

$$\{\boldsymbol{\tau}_i\}_j \cdot \left(\Delta \mathbf{d}_j - \sum_{l=1}^{n_m^e} N_l \Big|_{\mathbf{x}_j^m} \Delta \mathbf{d}_l \right) = 0, \quad \forall \{j \in \check{T}\}, \quad (9c)$$

$$z_j^{\tau_i} = -\mu |z_j^n| \{ \boldsymbol{\tau}_i \}_j \cdot \bar{\mathbf{v}}_{\tau} / \| \bar{\mathbf{v}}_{\tau} \|, \quad \forall \{ j \in \check{\mathcal{L}} \}, \quad (9d)$$

where n_m^e is the number of nodes per element on the master surface, $\circ g$ is the prescribed gap for the nodal discrete version of the gap function in the normal direction, N_l is the shape function of the master element, with regard to the current approximate configuration of projection \mathbf{x}^m , and subscript i can be 1 or 2.

Herein, we have briefly introduced the contact constraints after employing PDASS. Further details on PDASS can be found in Hüeber and Wohlmuth (2005). According to Hüeber and Wohlmuth (2005), the following system of equations can be obtained from Eq. (4):

$$\begin{bmatrix} \mathbf{K} & \begin{matrix} \mathbf{0} \\ -\mathbf{H}_M^T \\ \mathbf{H}_S^T \end{matrix} \\ \mathbf{0} & \begin{matrix} * & * \\ * & * \end{matrix} \end{bmatrix} \begin{bmatrix} \mathbf{d}_{\check{\mathcal{R}}} \\ \mathbf{d}_{\check{\mathcal{M}}} \\ \mathbf{d}_{\check{\mathcal{S}}} \\ \mathbf{z} \end{bmatrix} = \begin{bmatrix} \mathbf{F}_R^{\text{ext}} \\ \mathbf{F}_M^{\text{ext}} \\ \mathbf{F}_S^{\text{ext}} \\ * \end{bmatrix} \quad (10)$$

where stiffness matrix \mathbf{K} and external forces \mathbf{F}^{ext} are determined by partial derivative $\delta \Pi^{\text{int,ext}} / \delta \mathbf{d}$, and symbol * denotes the discrete contact constraints given by Eq. (9). Coefficient matrix \mathbf{H} is given by

$$\mathbf{H}_M = \int_{\Gamma^C} \Psi^T \mathbf{N}_M d\Gamma, \quad \mathbf{H}_S = \int_{\Gamma^C} \Psi^T \mathbf{N}_S d\Gamma \quad (11)$$

It should be noted that Eq. (9) can be inserted into Eq. (10) to obtain a complete expression. However, such an expression should be quite lengthy. As a result, a new generalized NTS formulation will be proposed in Section 3 by rewriting Eq. (9) into a decoupled form. Using this form, it is guaranteed that the contact constraints can be imposed just like imposing conventional boundary condition, rather than inserting Eq. (9) into Eq. (10). Hence, the complete expression is not given here and interested readers can refer to the dual mortar approach in Wohlmuth and Krause (2003), Hüeber and Wohlmuth (2005), and/or Sitzmann et al. (2014).

3. New generalized node-to-segment formulation

In this paper, an equivalent contact interface is proposed to solve the soft joint contact problem. As shown in Fig. 4, the extrusion displacement (u_n) of the filler is converted to penetration ($-g$), while the contact traction (p_n) on the interface is equivalent to the extrusion stress (σ_n):

$$u_n = -g, \quad \sigma_n = p_n. \quad (12)$$

In Section 2, the Lagrange multiplier method is employed to impose the contact constraints; the normal constraints are

under non-penetration conditions. This hard contact model cannot simulate the equivalent contact interface which should introduce penetration to represent the extrusion displacement. By employing the penalty method to impose the contact constraints, the penalty factor can result in penetration; and thus, the soft joint contact problem can be solved. However, the penalty method has the deficiency of leading to an ill-conditioned matrix system, and this severely reduces the efficiency when solving the matrix system, especially for large-scale contact problems.

To solve soft joint contact problems with high efficiency, we propose a new generalized NTS formulation based on the introduction of a general transformation and the application of the perturbed Lagrange method.

3.1. A general transformation

The optimization problem (Eq. (10)) with contact constraints (Eq. (9)) is a saddle-point problem, in which the Lagrange multipliers are primary unknowns leading to the increase in system size. To condense the Lagrange multipliers and to obtain a positive definite system, Wohlmuth and Krause (2003) and Sitzmann et al. (2014) introduced a local basis transformation for the dual mortar approach, and their transformation can result in point-wise decoupled contact constraints. Here we propose a more general transformation for the NTS approach. The transformation proposed in this paper can obtain fully decoupled contact constraints for each generalized displacement degree of freedom, rather than only point-wise decoupled contact constraints.

Firstly, we introduce the following expression:

$$\begin{aligned} \mathbf{z}_j^R &= [z_j^{\tau_1} \ z_j^{\tau_2} \ z_j^n]^T, \quad \bar{\mathbf{d}}_j^R = [\bar{d}_j^{\tau_1} \ \bar{d}_j^{\tau_2} \ \bar{d}_j^n]^T, \\ \mathbf{C}_{jl} &= N_l \Big|_{\mathbf{x}_j^m} \mathbf{I}_3, \quad \mathbf{R}_{jk} = \delta_{jk} \begin{bmatrix} (\boldsymbol{\tau}_1)_j & (\boldsymbol{\tau}_2)_j & \mathbf{n}_j \end{bmatrix}, \quad \forall \{ j, k \in \check{\mathcal{A}}, l \in \check{\mathcal{M}} \}, \end{aligned} \quad (13)$$

where the rotated Lagrange multipliers \mathbf{z}_j^R are defined in the local coordinate system composed of the unit tangential and normal vectors, generalized displacements $\bar{\mathbf{d}}_j^R$ represent the relative displacements in the local coordinate system, defined as the difference in displacement between the slave nodes and their master nodes, matrix \mathbf{C} describes the relation between master and slave sides, and matrix \mathbf{R} represents the orthogonal transformation from the global coordinate system to the local coordinate system.

By comparing the expression of Eqs. (8) and (9) with the definitions of \mathbf{z}_j^R and $\bar{\mathbf{d}}_j^R$, respectively, \mathbf{z}_j^R and $\bar{\mathbf{d}}_j^R$ can be written

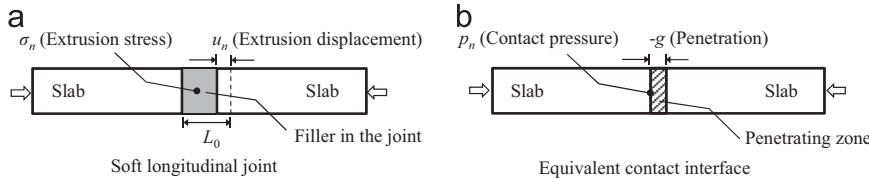


Fig. 4. Schematic of equivalent contact interface.

as

$$\mathbf{z}_j^R = [\mathbf{R}]_{jj}^T \mathbf{z}_j, \Delta \bar{\mathbf{d}}_j^R = [\mathbf{R}]_{jj}^T \left\{ \Delta \mathbf{d}_j - \sum_{l \in \check{\mathcal{M}}} \mathbf{C}_{jl} \Delta \mathbf{d}_l \right\}, \quad \forall \{j \in \check{\mathcal{A}}\}. \quad (14)$$

By omitting the contact constraints temporarily, the incremental form of Eq. (10) can be written as

$$\mathbf{K} \Delta \mathbf{d} = \mathbf{r}, \quad \mathbf{r} = \mathbf{F}^{\text{ext}} - \mathbf{F}^{\text{int}} + \mathbf{F}^C = \mathbf{F}^{\text{int,ext}} + \mathbf{F}^C, \quad (15)$$

where \mathbf{r} is the residual force vector, \mathbf{F}^{int} and \mathbf{F}^{ext} denote the internal and external forces, respectively, symbol $\mathbf{F}^{\text{int,ext}}$ denotes $\mathbf{F}^{\text{ext}} - \mathbf{F}^{\text{int}}$, and contact force \mathbf{F}^C is defined by the partial derivative $\delta \Pi_u^C / \delta \mathbf{d}$. It can be written as

$$\mathbf{F}_M^C = \mathbf{H}_M^T \mathbf{z}, \quad \mathbf{F}_S^C = -\mathbf{H}_S^T \mathbf{z}. \quad (16)$$

It can be seen that the Lagrange multipliers are rewritten in the contact force \mathbf{F}^C . Then, we introduce the general transformation as a matrix \mathbf{P} , namely,

$$\mathbf{P} = \begin{bmatrix} \mathbf{I}_{RR} & \mathbf{0} & \mathbf{0} & \mathbf{0} \\ \mathbf{0} & \mathbf{I}_{MM} & \mathbf{0} & \mathbf{0} \\ \mathbf{0} & \mathbf{0} & \mathbf{I}_{II} & \mathbf{0} \\ \mathbf{0} & \mathbf{0} & \mathbf{C} & \mathbf{R} \end{bmatrix}. \quad (17)$$

Therefore, we can propose the transformed system of equations as

$$\tilde{\mathbf{K}} \Delta \tilde{\mathbf{d}} = \tilde{\mathbf{r}}, \quad \text{with}$$

$$\tilde{\mathbf{K}} = \mathbf{P}^T \mathbf{K} \mathbf{P},$$

$$\begin{aligned} \mathbf{P} \Delta \tilde{\mathbf{d}} &= \Delta \mathbf{d}, \quad \Delta \tilde{\mathbf{d}} = \left[\Delta \mathbf{d}_R^T \quad \Delta \mathbf{d}_M^T \quad \Delta \mathbf{d}_I^T \quad \Delta \bar{\mathbf{d}}_A^R \right]^T, \\ \tilde{\mathbf{r}} &= \mathbf{P}^T \mathbf{r} = \left[\mathbf{r}_R^T \quad \mathbf{F}_M^{\text{int,ext}} + \mathbf{C}^T \mathbf{F}_A^{\text{int,ext}} \quad \mathbf{r}_I^T \quad \mathbf{R}^T \mathbf{F}_A^{\text{int,ext}} - \mathbf{H}_A^T \mathbf{z}_A^R \right]^T, \end{aligned} \quad (18)$$

where rotated Lagrange multipliers \mathbf{z}_j^R and generalized displacements $\bar{\mathbf{d}}_j^R$ form duality pairings. Applying these duality pairings to express the contact constraints of the active slave nodes, the Lagrange multiplier formulation can be written as follows:

$$\begin{cases} \mathbf{z}_j = \mathbf{0}, \quad \forall \{j \in \check{\mathcal{I}}\}, \\ \Delta \bar{d}_j^n = -\bar{d}_j^n, \quad \forall \{j \in \check{\mathcal{A}}\}, \\ \Delta \bar{d}_j^{t_i} = 0, \quad i = \{1, 2\}, \quad \forall \{j \in \check{\mathcal{T}}\}, \\ z_j^{t_i} = -\mu |z_j^n| \{ \mathbf{t}_i \}_j \cdot \bar{\mathbf{v}}_\tau / \| \bar{\mathbf{v}}_\tau \|, \quad i = \{1, 2\}, \quad \forall \{j \in \check{\mathcal{L}}\}, \end{cases} \quad (19)$$

As can be seen from Eq. (19), we obtain fully decoupled contact constraints for each generalized displacement degree of freedom. Therefore, the Lagrange multipliers are condensed and the resulting matrix system is positive definite.

3.2. Perturbed Lagrange formulation

The Lagrange multiplier formulation (Eq. (19)) provides significant convenience when applying the perturbed Lagrange method to solve soft contact problems. According to Sitzmann

et al. (2014), the normal contact constraints in the perturbed Lagrange formulation can be written as

$$z_j^n = \tilde{\alpha} g_j^h, \quad \forall \{j \in \check{\mathcal{S}}\}, \quad (20)$$

where z_j^n is the nodal normal contact traction, $\tilde{\alpha}$ is the penalty factor, and g_j^h denotes the nodal normal gap. Shape function ψ in the Lagrange multipliers can be taken as the dual basis function which satisfies the following biorthogonal condition (Scott and Zhang, 1990):

$$\int_{\Gamma^C} \psi_j N_k d\Gamma = \delta_{jk} \int_{\Gamma^C} N_k d\Gamma, \quad \forall \{j, k \in \check{\mathcal{S}}\}, \quad (21)$$

Inserting Eqs. (20) and (21) into Eq. (16), contact forces F_j^n can be written as

$$F_j^n = -z_j^n \sum_{k \in \check{\mathcal{S}}} \int_{\Gamma^C} \psi_j N_k d\Gamma = -\tilde{\alpha} g_j^h \int_{\Gamma^C} N_k d\Gamma, \quad \forall \{j \in \check{\mathcal{S}}\}, \quad (22)$$

By introducing equivalent nodal area S_j , Eq. (22) is rewritten as

$$S_j = \int_{\Gamma^C} N_j d\Gamma, \quad F_j^n = -S_j \tilde{\alpha} g_j^h, \quad \forall \{j \in \check{\mathcal{S}}\}, \quad (23)$$

where S_j represents the nodal contact force per unit contact traction, and penalty factor $\tilde{\alpha}$ represents the value of the contact stiffness per unit nodal area S_j .

Then, we apply our proposed general transformation to derive the perturbed Lagrange formulation as

$$\begin{cases} (\tilde{\mathbf{K}} + \mathbf{Q}) \Delta \tilde{\mathbf{d}} = \tilde{\mathbf{r}}, \\ \mathbf{z}_j = \mathbf{0}, \quad \forall \{j \in \check{\mathcal{I}}\}, \\ \Delta \bar{d}_j^n = 0, \quad i = \{1, 2\}, \quad \forall \{j \in \check{\mathcal{T}}\}, \\ z_j^{t_i} = -\mu |z_j^n| \{ \mathbf{t}_i \}_j \cdot \bar{\mathbf{v}}_\tau / \| \bar{\mathbf{v}}_\tau \|, \quad i = \{1, 2\}, \quad \forall \{j \in \check{\mathcal{L}}\}, \end{cases} \quad (24)$$

where matrix \mathbf{Q} is defined as

$$\mathbf{Q}_{jk} = \delta_{jk} \begin{bmatrix} 0 & 0 & 0 \\ 0 & 0 & 0 \\ 0 & 0 & S_j \tilde{\alpha} \end{bmatrix}, \quad \forall \{j, k \in \check{\mathcal{A}}\}. \quad (25)$$

As can be seen from Eqs. (24) and (25), the fully decoupled contact constraints guarantee that penalty factor $\tilde{\alpha}$ is only involved in the diagonal position of the matrix system $(\tilde{\mathbf{K}} + \mathbf{Q})$, and thus, the ill-condition is overcome.

Based on the above work, we obtain a new generalized NTS formulation, including the Lagrange multiplier formulation (Eq. (19)) for hard contact problems and the perturbed Lagrange formulation (Eq. (24)) for soft contact problems.

3.3. Estimation of penalty factor

To simulate the closing state of soft joints, penalty factor $\tilde{\alpha}$ should change with penetration g_j^h . That is, after a certain amount of penetration occurs, the subsequent penetration is assumed to be very small. Here we provide a convenient estimation of the penalty factor.

For the filler material, extrusion strain ϵ_n and extrusion modulus E_n are defined as

$$\epsilon_n = \frac{u_n}{L_0}, \quad E_n = \frac{\Delta\sigma_n}{\Delta\epsilon_n}, \quad (26)$$

where u_n , L_0 , and σ_n are the extrusion displacement, the initial width, and the extrusion stress of the filler, respectively. Inserting Eq. (12) into Eq. (26) yields

$$\Delta p_n = \Delta\sigma_n = E_n \Delta\epsilon_n = E_n \frac{\Delta u_n}{L_0} = -E_n \frac{\Delta g}{L_0}, \quad (27)$$

Comparing Eq. (20) with Eq. (27), the penalty factor can be written as

$$\tilde{\alpha} = E_n/L_0, \quad \forall \{j \in \check{S}\}, \quad (28)$$

Eq. (28) can provide a reliable estimation of the penalty factor because extrusion modulus E_n can be determined by compression test results. For simplicity, a bilinear extrusion model is assumed here for extrusion modulus E_n :

$$\begin{cases} E_n = E_{n1}, & \text{when } \epsilon_n \leq \epsilon_n^c, \\ E_n = E_{n2}, & \text{when } \epsilon_n > \epsilon_n^c, \end{cases} \quad (29)$$

where critical extrusion strain ϵ_n^c means that the maximum extrusion displacement that can be absorbed by the soft joints is about $\epsilon_n^c \cdot L_0$. Therefore, before and after the penetration reaches the critical value of $\epsilon_n^c \cdot L_0$, penalty factor $\tilde{\alpha}$ is taken as E_{n1}/L_0 and E_{n2}/L_0 , respectively.

In this simplified model, extrusion modulus E_{n1} is employed to describe the effect of absorbing extrusion deformation, while E_{n2} is adopted to describe the closing state. As mentioned in Section 1, the purpose of using soft filler is to avoid extrusion damage. Therefore, although this simplified model cannot include all the details for describing the soft filler, it can capture some fundamental features that may be of concern, such as absorbing extrusion deformation and reaching the closing state.

When dealing with the test data, we can appropriately pick a data point corresponding to critical extrusion strain ϵ_n^c . Here, a simple method is introduced below. Firstly, we can define E_{n1} and E_{n2} as the average modulus before and after critical strain ϵ_n^c , respectively. Then, ϵ_n^c can be determined by making E_{n2} large enough to ensure that the subsequent penetration is small, since E_{n2} represents the closing state.

3.4. An example

To verify the proposed new generalized NTS formulation and to demonstrate its numerical implementation, the three-dimensional contact patch test is simulated. The right part in Fig. 5 presents two concrete cubes with a unit length (1 m). For both cubes, a linear elastic material with Young's modulus $E=30,000$ MPa and Poisson's ratio $\nu=0$ is applied. The upper block is chosen as the master side. The contact interface is the equivalent interface of the soft joint, and the parameters of the bilinear extrusion model are taken as $L_0=16$ mm, $E_{n1}=5$ MPa, $\epsilon_n^c=0.5$, and $E_{n2}=30,000$ MPa, which leads to a critical penetration of 8 mm.

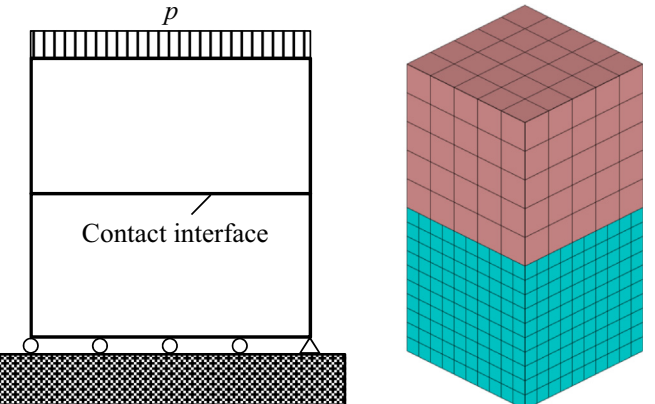


Fig. 5. Contact patch test and three-dimensional mesh.

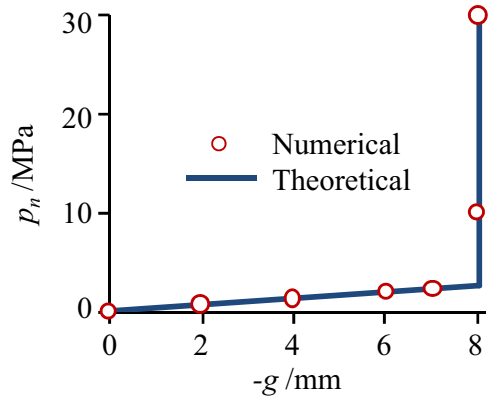


Fig. 6. Contact traction (p_n) vs. penetration ($-g$).

In the simulation, pressure p is increased at six loading steps of 0.625, 1.250, 1.875, 2.2, 10, and 30 MPa, respectively. The theoretical results of this problem give a constant stress distribution with the contact traction of p . In the obtained results, the penetration and the contact traction on the interface are uniform at each loading step. Fig. 6 shows the relation between the contact traction (p_n) and the penetration ($-g$), with a good agreement between the numerical solution and the theoretical results.

4. Numerical analysis of TSQ-1 CFRD

The TSQ-1 project is located at the Nanpan River in southwestern China. Its total storage capacity is 10.257 billion m³ and the total installed capacity is 1200 MW. The water retaining structure is a concrete-faced rockfill dam with a height of 178 m and an axial length of 1104 m. This dam was the first super-high CFRD constructed in China. The rockfill volume of the dam body was about 18 million m³. The upstream and downstream slopes are 1:1.4 and 1:1.25, respectively. The concrete faces consist of 69 slabs. Each slab is 16 m wide with a variable thickness, which decreases linearly from 0.9 m at the bottom elevation of 616.5–0.3 m at the top elevation of 787.3 m.

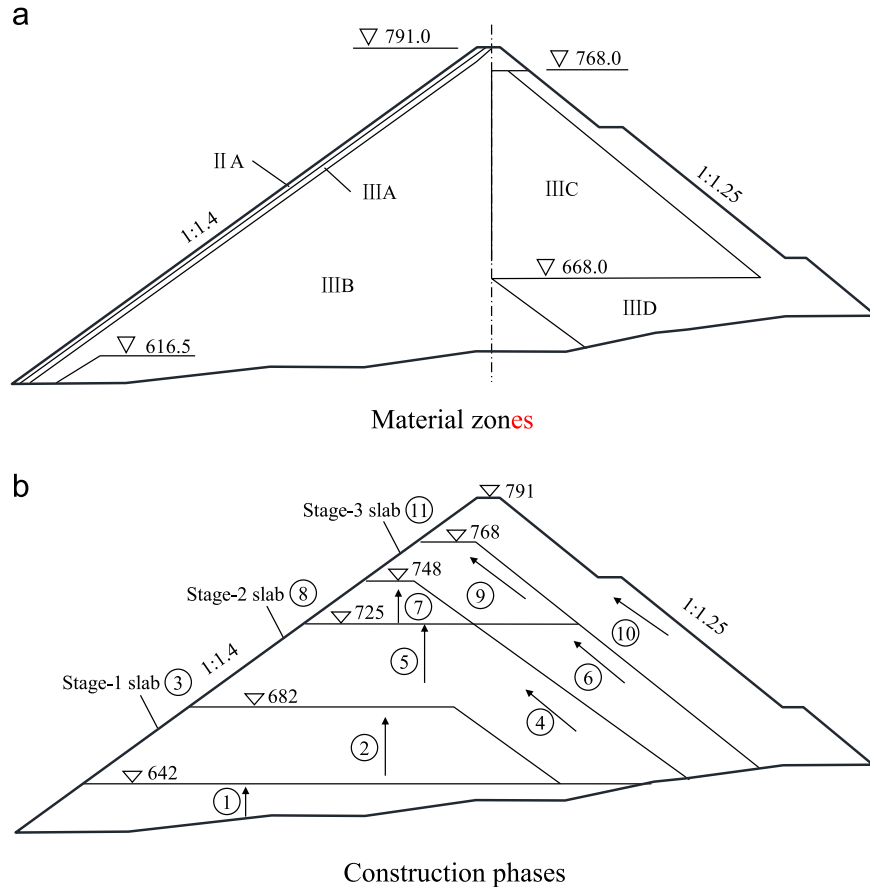


Fig. 7. Material zones and construction phases of TSQ-1 CFRD.

Fig. 7a shows the material zones in a typical cross-section. The rockfill body is divided into five zones: bedding zone IIA, which performs as the cushion layer, transition zone IIIA, upstream rockfill zone IIIB, mudstone and sandstone zone IIIC, and downstream rockfill zone IID. **Fig. 7b** shows the construction phases. The filling of the rockfill body commenced in February 1996 and was completed in March 1999. The construction of the slabs commenced in March 1997 and was completed in May 1999. The slabs were cast in three phases at top elevations of 680 m, 746 m, and 787.3 m, respectively.

The dam operated safely for about 13 years. However, extrusion damage in the face slabs was first discovered at joint LJ3 in July 2003. Subsequently, in 2004, 2005, 2008, 2009, 2011, and 2012, similar extrusion damage continued to appear, mainly occurring at joints LJ3 and LJ8 (red lines in **Fig. 8**).

In the simulation of this problem, the external loads include the self-weight of the dam and the water pressure on the concrete face. In the operating period without serious damage, the concrete face can be assumed to be impermeable; and thus, the seepage can be ignored in the simulation. Moreover, the TSQ-1 CFRD is constructed on the hard rock with high modulus and the valley in this project is as wide as 1104 m, so the contact between the dam and the foundation can be simplified by fixing the displacements at the bottom of the dam as zero. The numerical analysis of the TSQ-1 CFRD was

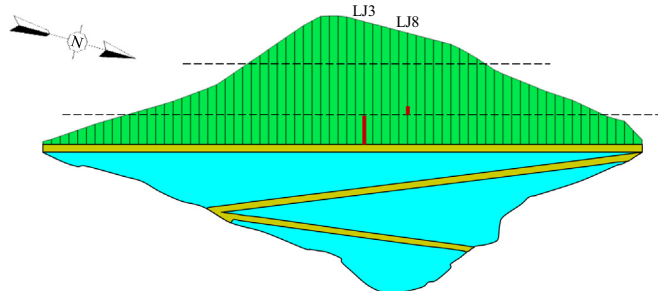


Fig. 8. Schematics of damage position of face slabs. (For interpretation of the references to color in this figure, the reader is referred to the web version of this article.)

implemented by considering the rockfill body, the cushion layer, and the face slabs as individual contact bodies. **Fig. 9** shows the 3D mesh with 27,257 nodes and 17,299 elements. In order to reduce the computing costs without losing the numerical precision, a coarse mesh was used for the rockfill body, while finer meshes were used for the cushion layer and the face slabs. **Fig. 10** shows the mesh on the right bank with the finer details in the insert. The insert shows the relation between the different contact bodies. The face slabs were modeled with 69 contact bodies.

The rockfill materials are modeled by Duncan and Chang's E-B model (Duncan et al., 1980). Deformation modulus E_t and

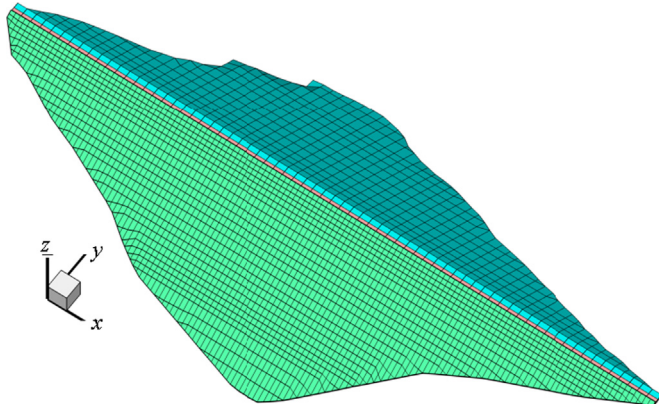


Fig. 9. Mesh for numerical analysis of TSQ-1 CFRD.

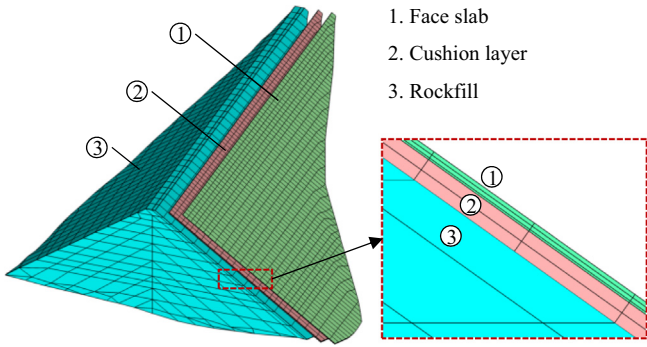


Fig. 10. Contact relations for slab, cushion, and rockfill.

bulk modulus B are given by

$$E_t = k \cdot P_a (\sigma_3/P_a)^n \cdot \left(1 - R_f \frac{(1 - \sin \phi)(\sigma_1 - \sigma_3)}{2c \cdot \cos \phi + 2\sigma_3 \sin \phi}\right)^2, \quad (30)$$

$$B = k_b P_a (\sigma_3/P_a)^m,$$

where k , n , R_f , c , ϕ , k_b , and m are material parameters, P_a is the atmospheric pressure, and σ_i and $(\sigma_1 - \sigma_3)$ denote the i th principal stress and the deviatoric stress, respectively. For the rockfill, c is taken as zero while ϕ changes with pressure.

$$\varphi = \varphi_0 - \Delta\varphi \log(\sigma_3/P_a), \quad (31)$$

where φ_0 and $\Delta\varphi$ are the soil strength constants.

The creep model for rockfill materials used in this paper employs an empirical scheme (Li et al., 2004). The rate of the creep strain is given by

$$\dot{\varepsilon}_{vt} = \alpha_c \varepsilon_{vf} (1 - \varepsilon_{vt}/\varepsilon_{vf}), \quad \dot{\varepsilon}_{st} = \alpha_c \varepsilon_{sf} (1 - \varepsilon_{st}/\varepsilon_{sf}),$$

$$\varepsilon_{vf} = b_c (\sigma_3/P_a)^{m_c} + \beta_c (\sigma_s/P_a)^{n_c}, \quad \varepsilon_{sf} = d_c [S_L/(1 - S_L)]^{L_c}, \quad (32)$$

where ε_f is the ultimate total creep strain. α_c , b_c , m_c , β_c , n_c , d_c , and L_c are material parameters. Equivalent stress σ_s and shear stress level S_L are defined as follows:

$$\sigma_s = \frac{1}{\sqrt{2}} \sqrt{(\sigma_1 - \sigma_2)^2 + (\sigma_2 - \sigma_3)^2 + (\sigma_3 - \sigma_1)^2}, \quad (33)$$

$$S_L = \frac{(1 - \sin \phi)(\sigma_1 - \sigma_3)}{2c \cdot \cos \phi + 2\sigma_3 \sin \phi},$$

Table 1
Parameters for the E-B model.

Material No.	ϕ_0 (°)	$\Delta\phi$ (°)	k	n	R_f	k_b	m
IIA	50.6	7.0	720	0.30	0.71	300	0.20
IIIA	52.5	8.0	720	0.30	0.76	300	0.20
IIIB	54.0	13.0	443	0.236	0.85	290	0.158
IIIC	48.0	10.0	295	0.198	0.73	108	0.030
IID	54.0	13.5	323	0.247	0.80	132	0.030

Table 2
Parameters for the creep model.

Material No.	α_c	b_c	d_c	m_c	β_c	n_c	L_c
IIA	0.00028	0.00048	0.0090	0.50	0.00042	0.50	0.51
IIIA	0.00028	0.00048	0.0090	0.50	0.00042	0.50	0.51
IIIB	0.00025	0.00061	0.0083	0.50	0.00024	0.50	0.51
IIIC	0.00080	0.00060	0.0083	0.50	0.00046	0.46	0.50
IID	0.00029	0.00104	0.0136	0.68	0.00039	0.59	0.64

In this simulation, the parameters for the E-B model and the creep model for rockfill materials are shown in Tables 1 and 2, respectively, which are determined by the three-dimensional (3D) back analysis based on the monitored deformation data. For TSQ-1 CFRD, Zhang et al. (2004) also conducted a two-dimensional (2D) back analysis to determine the model parameters. It should be noted that the parameters employed for the 2D and 3D simulations may be different. For the face slabs, a linear elastic material with Young's modulus $E=30,000$ MPa and Poisson's ratio $\nu=0.2$ is adopted. The cushion layer is tied to the rockfill body to simplify the mesh transition. For the slab–cushion contact, the tangential constraints are Coulomb's law with a frictional coefficient of $\mu=0.7$, and the normal constraints are taken as the hard contact model which can be treated by the Lagrange multiplier formulation proposed in this paper.

For the TSQ-1 project, soft joints were thought to be a promising engineering solution to prevent subsequent extrusion damage. To study the effect of soft joints, we simulate the following three cases for the slab–slab contact:

Case 1. the hard contact case without soft joints, which is the real case in the TSQ-1 project.

Case 2. the case employing 5 soft joints (see the red lines in Fig. 11a).

Case 3. the case employing 10 soft joints (see the red lines in Fig. 11b).

In these three cases, the tangential constraints of the slab–slab contact are Coulomb's law with a frictional coefficient of $\mu=0.7$. In Case 1, the normal constraints are taken as the hard contact model, and they are imposed by the Lagrange multiplier formulation proposed in this paper. In Cases 2 and 3, it was assumed that the soft joints were applied once the construction of the face slabs had been completed. The soft

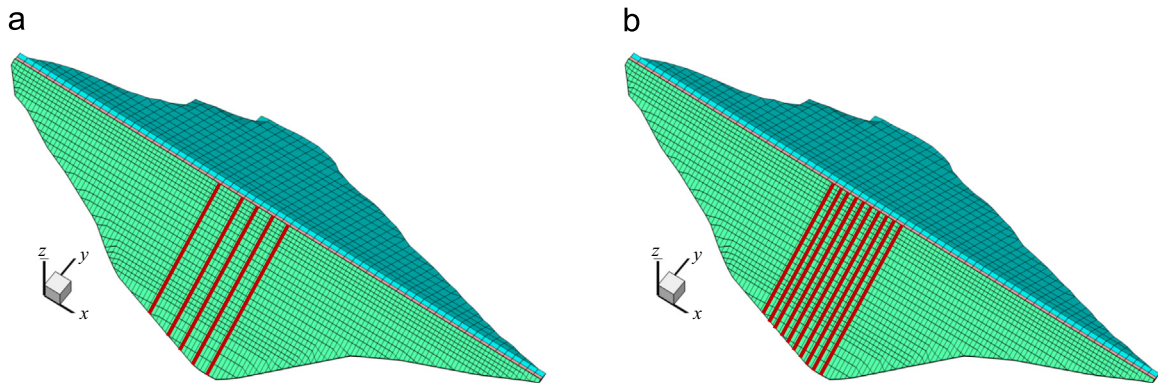


Fig. 11. Arrangement of soft joints. (a) 5 soft joints. (b) 10 soft joints. (For interpretation of the references to color in this figure, the reader is referred to the web version of this article.)

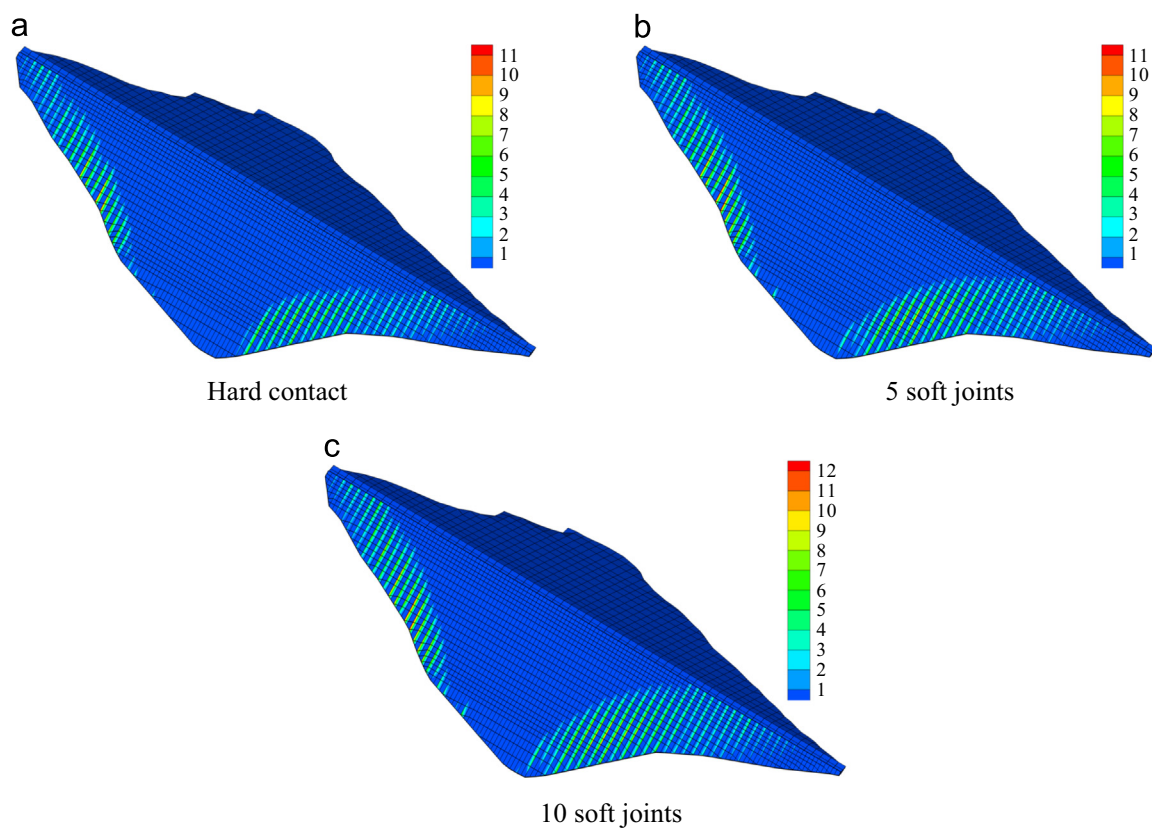


Fig. 12. Positive normal gap between face slabs (Unit: mm).

joints are treated as the equivalent soft contact interface, of which the normal constraints are imposed by the perturbed Lagrange formulation proposed in this paper. In the perturbed Lagrange formulation, the parameters of the bilinear extrusion model are the same as those in Section 3.4, which leads to a critical penetration of 8 mm.

The termination time of the numerical simulation was taken as July 2003 when the extrusion damage of the face slabs firstly occurred. The numerical results of the three cases on July 2003 are presented in Figs. 12–15. Fig. 12 shows the distribution of the positive normal gap (implying separation). The separation in the two cases employing soft joints (Cases 2 and 3) is slightly larger

than that in Case 1. The difference of the separation in the three cases is not significant, the reason is thought to be that the wide valley of the TSQ-1 project provides a good scope of adjustment for the axial deformation.

Fig. 13 shows the distribution of the negative normal gap (implying penetration) at the soft joints. The penetration is equivalent to the axial extrusion displacement absorbed by the soft joints. The maximum penetration at each soft joint is above 7 mm, almost reaching the critical value of 8 mm.

Fig. 14 shows the distribution of the axial stress on the surface of the slabs, and the positive value implies that the slabs are under extruding. A comparison of the three cases shows that the soft

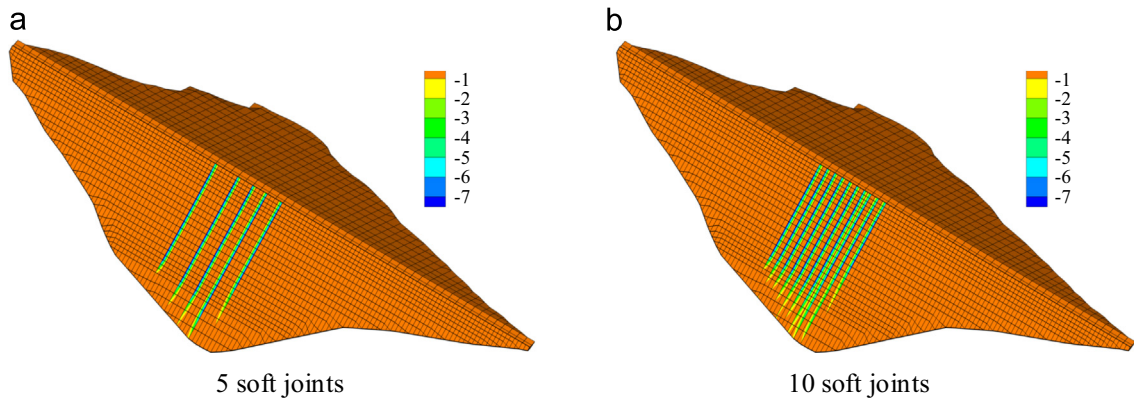


Fig. 13. Negative normal gap between face slabs (Unit: mm).

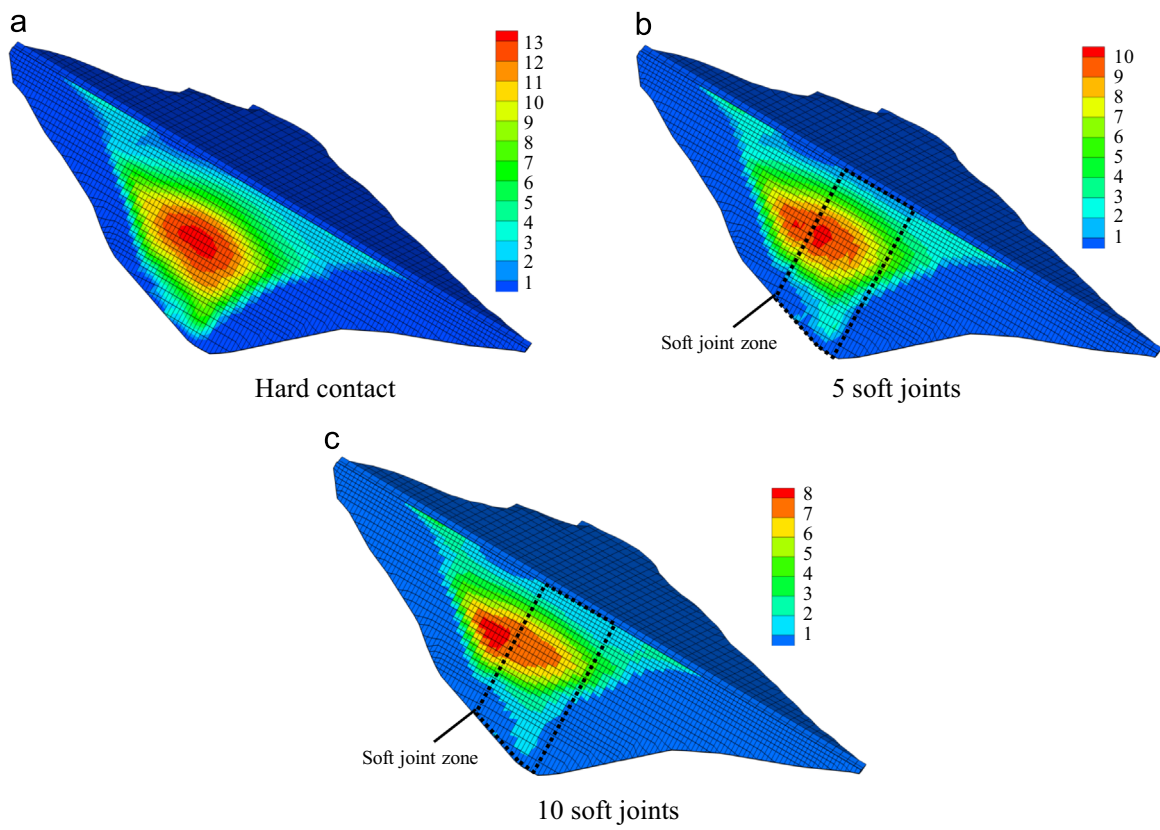


Fig. 14. Distribution of axial stress on surface of face slabs (Unit: MPa).

joints have a significant effect on the maximum extrusion stress of the face slabs. In the hard contact case (Case 1), the maximal extrusion stress is about 13 MPa (see Fig. 14a). In the two cases employing soft joints (Cases 2 and 3), the maximum levels of extrusion stress in the soft joint zone are about 9 MPa and 7 MPa, respectively, decreasing 23% and 46% in comparison with Case 1 (see Fig. 14b and c).

Fig. 15 shows the variation in axial stress at joint LJ3 (Fig. 8), where extrusion damage occurred in practice. It is obvious that the axial stress can be effectively reduced by using soft joints in the axial compressive zone of the face slabs.

5. Conclusions

The soft joint contact problem was considered as an equivalent soft contact interface in this paper to avoid the introduction of conventional elements when modeling a thin filler. A general transformation was presented to obtain fully decoupled contact constraints, and a new generalized node-to-segment formulation was proposed.

This new formulation, including the Lagrange multiplier formulation and the perturbed Lagrange formulation, provides a general and convenient framework for solving the multi-body

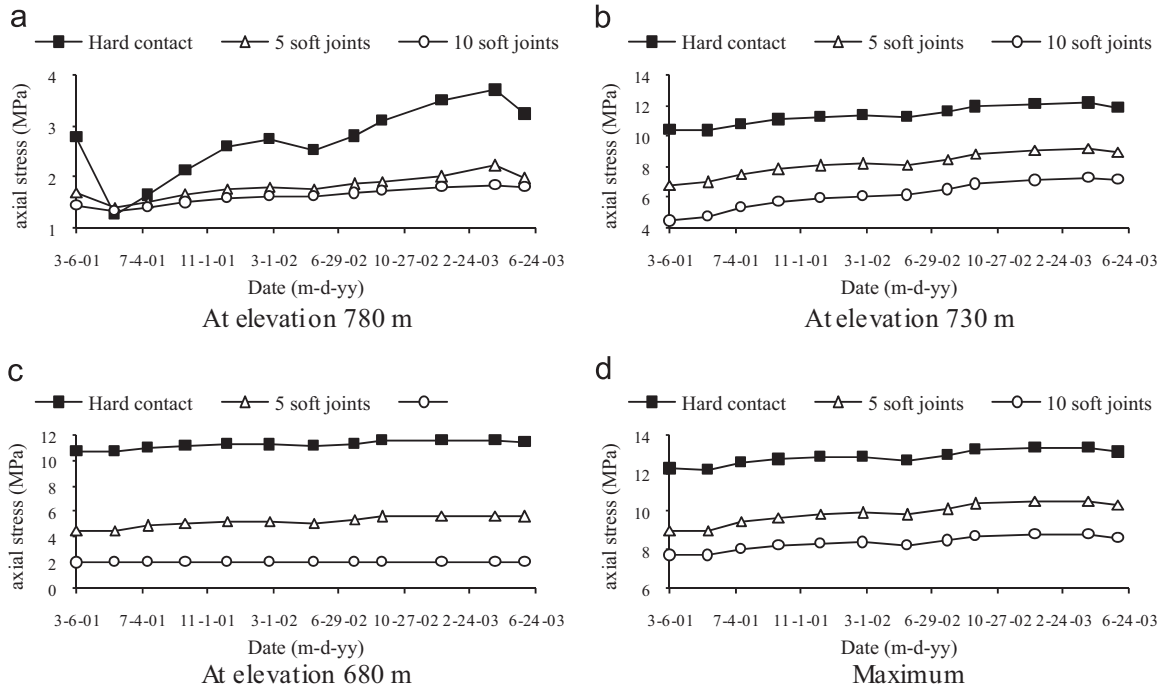


Fig. 15. Variation in axial stress.

contact problem in CFRD projects, especially when a hard contact model and a soft contact model are both involved in the simulation. The Lagrange multiplier formulation, resulting in a positive definite matrix system, can be used to simulate the hard contact model, which is the conventional case in CFRD. The perturbed Lagrange formulation, whose application prevents an ill-conditioned matrix system, can be used to simulate the soft contact model.

We performed a numerical simulation of the Tianshengqiao-1 CFRD. The numerical results in three cases, a real case without soft joints and two cases with soft joints, were compared. The maximum penetration at each soft joint almost reached the critical value, which represented the extreme extrusion displacement that can be absorbed by the soft joints. It was found that employing the soft joints in the compressive zone can effectively reduce the axial stress of the face slabs.

In this paper, we mainly studied the numerical analysis method and engineering effect of soft joints, and results show that its application will be promising in preventing extrusion damage to the concrete face. However, the cause of practical extrusion damage is complicated and is not totally explained here. Based on the present work on the computational contact analysis, comprehensive factors will be taken into account to study the cause of extrusion damage in our future work.

Acknowledgments

The authors would like to acknowledge the financial support of the Natural Science Foundation of China, Grant nos. 51479099 and 51279085, and the Project of Zhongtiaoshan Tunnel of Mengxi Railway.

References

- Arici, Y., 2011. Investigation of the cracking of CFRD face plates. *Comput. Geotech.* 38 (7), 905–916.
- Cao, K.M., Zhang, Z.L., 2001. Performance of the Tianshengqiao 1 CFRD. *Int. J. Hydropower Dams* 8 (5), 78–83.
- Cao, K.M., Xu, J.J., 2009. Discussions on critical deflection of face slab and its design improvement for super-high CFRD. *Water Power* 34 (11), 98–102 in Chinese.
- Cooke, J.B., 1991. Concrete-faced rockfill dam. *Int. Water Power Dam Constr.* 43 (1), 11–15.
- Desai, C.S., Lightner, J.G., Siriwardane, H.J., Zaman, M.M., 1984. Thin-layer element for interfaces and joints. *Int. J. Numer. Anal. Methods Geomech.* 8 (1), 19–43.
- Duncan, J.M., Byrne, P., Wong, K., Mabry, P., 1980. Strength, Stress–Strain and Bulk Modulus Parameters for Finite Element Analysis of Stresses and Movements in Soil Masses. University of California, Berkeley.
- Goodman, R.E., Taylor, R.L., Brekke, T.L., 1968. A model for the mechanics of jointed rock. *J. Soil. Mech. Found. Div. ASCE* 94 (SM3), 637–659.
- Hüeber, S., Wohlmuth, B.I., 2005. A primal-dual active set strategy for nonlinear multibody contact problems. *Comp. Methods Appl. Mech. Eng.* 194 (27), 3147–3166.
- Hallquist, J.O., Goudreau, G.L., Benson, D.J., 1985. Sliding interfaces with contact–impact in large-scale Lagrangian computations. *Comput. Methods Appl. Mech. Eng.* 51 (1), 107–137.
- Johannesson, P., Tohlang, S.L., 2007. Lessons learned from Mohale. *Int. Water Power Dam Constr.* 59 (8), 16–25.
- Kartal, M.E., Bayraktar, A., Başağa, H.B., 2012. Nonlinear finite element reliability analysis of concrete-faced rockfill (CFR) dams under static effects. *Appl. Math. Model.* 36 (11), 5229–5248.
- Li, G.Y., Mi, Z.K., Fu, H., 2004. Experimental studies on rheological behaviors for rockfills in concrete faced rockfill dam. *Rock Soil Mech.* 25 (11), 1712–1716 in Chinese.
- Li, N.H., Yang, Z.Y., 2012. Technical advances in concrete face rockfill dams in China. *Chin. J. Geotech. Eng.* 34 (8), 1361–1368 in Chinese.
- Popp, A., Wall, W.A., 2014. Dual mortar methods for computational contact mechanics—overview and recent developments. *GAMM – Mitt.* 37 (1), 66–84.

- Qian, X., Yuan, H., Li, Q., Zhang, B., 2013. Comparative study on interface elements, thin-layer elements and contact analysis methods in the analysis of high concrete-faced rockfill dams. *J. Appl. Math.* (19), 4499–4588.
- Scott, L.R., Zhang, S., 1990. Finite element interpolation of nonsmooth functions satisfying boundary conditions. *Math. Comput.* 54 (190), 483–493.
- Sheng, D., Sun, D.A., Matsuoka, H., 2006. Cantilever sheet-pile wall modelled by frictional contact. *Soils Found.* 46 (1), 29–37.
- Sitzmann, S., Willner, K., Wohlmuth, B.I., 2014. A dual Lagrange method for contact problems with regularized contact conditions. *Int. J. Numer. Methods Eng.* 99 (3), 221–238.
- Wohlmuth, B.I., Krause, R.H., 2003. Monotone multigrid methods on nonmatching grids for nonlinear multibody contact problems. *SIAM J. Sci. Comput.* 25 (1), 324–347.
- Xu, B., Zou, D., Liu, H., 2012. Three-dimensional simulation of the construction process of the Zipingpu concrete face rockfill dam based on a generalized plasticity model. *Comput. Geotech.* 43, 143–154.
- Zavarise, G., Wriggers, P., 1998. A segment-to-segment contact strategy. *Math. Comput. Model.* 28 (4), 497–515.
- Zavarise, G., Wriggers, P., Schrefler, B.A., 1995. On augmented Lagrangian algorithms for thermomechanical contact problems with friction. *Int. J. Numer. Methods Eng.* 38 (17), 2929–2949.
- Zhang, B., Wang, J.G., Shi, R., 2004. Time-dependent deformation in high concrete-faced rockfill dam and separation between concrete face slab and cushion layer. *Comput. Geotech.* 31 (7), 559–573.
- Zhang, G., Zhang, J.M., Yu, Y., 2007. Modeling of gravelly soil with multiple lithologic components and its application. *Soils Found.* 47 (4), 799–810.